Volume 16 | Number 26 | 14 July 2014 | Pages 12989–13542

PCCP

Physical Chemistry Chemical Physics

www.rsc.org/pccp

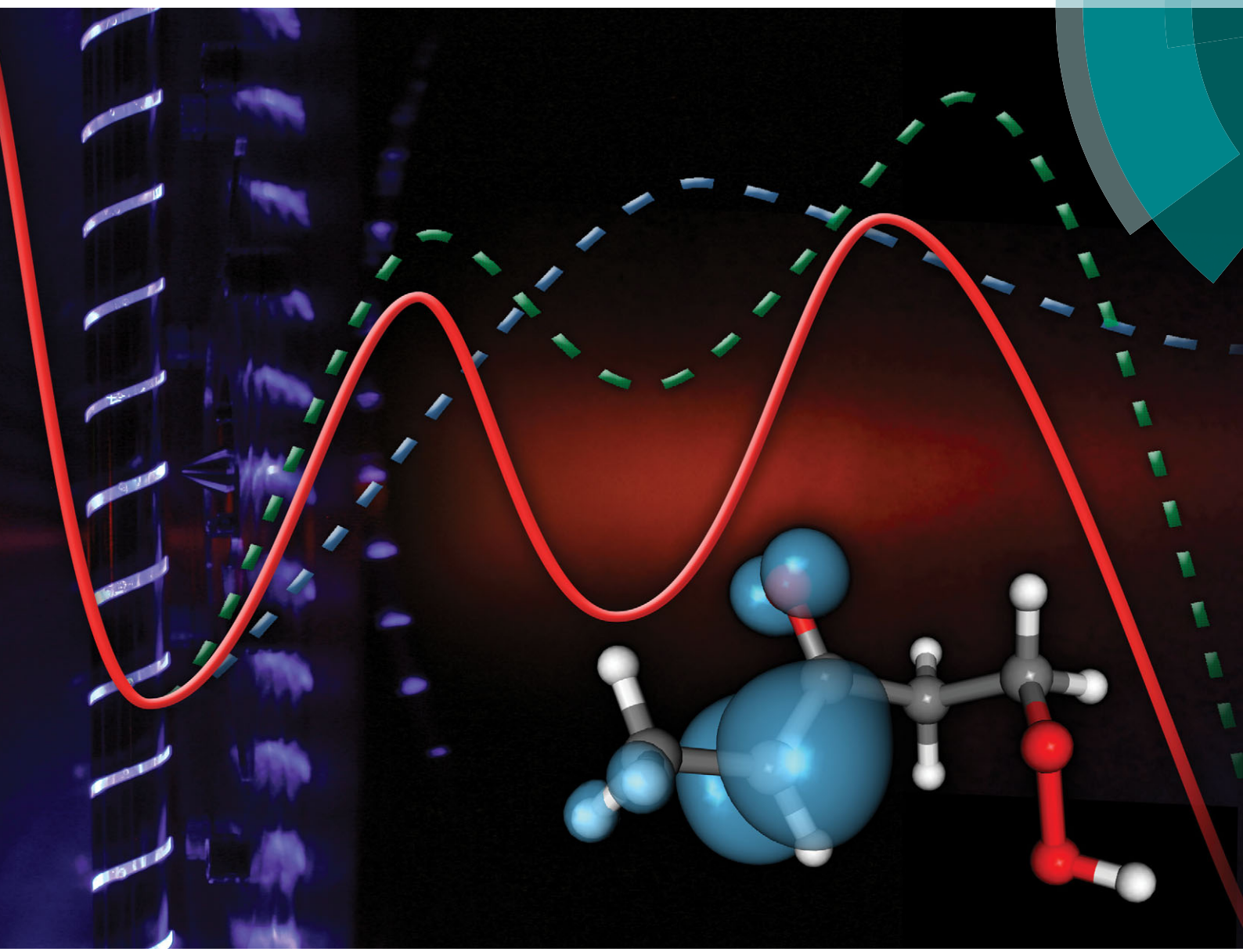

ISSN 1463-9076

ROYAL SOCIETY OF CHEMISTRY

PAPER

Craig A. Taatjes *et al.*

Low-temperature combustion chemistry of novel biofuels: resonance-stabilized QOOH in the oxidation of diethyl ketone

PCCP

PAPER

View Article Online
View Journal | View Issue

Cite this: *Phys. Chem. Chem. Phys.*, 2014, **16**, 13027

Low-temperature combustion chemistry of novel biofuels: resonance-stabilized QOOH in the oxidation of diethyl ketone†

Adam M. Scheer, Oliver Welz, Judit Zádor, David L. Osborn and Craig A. Taatjes*

Received 27th December 2013,
Accepted 14th February 2014

DOI: 10.1039/c3cp55468f

www.rsc.org/pccp

The $Cl^{\bullet}$ initiated oxidation reactions of diethyl ketone (DEK; 3-pentanone; $(CH_3CH_2)_2C{=}O$), 2,2,4,4-d_4-diethyl ketone (d_4-DEK; $(CH_3CD_2)_2C{=}O$) and 1,1,1,5,5,5-d_6-diethyl ketone (d_6-DEK; $(CD_3CH_2)_2C{=}O$) are studied at 8 Torr and 550–650 K using Cl_2 as a source for the pulsed-photolytic generation of $Cl^{\bullet}$. Products are monitored as a function of reaction time, mass, and photoionization energy using multiplexed photoionization mass spectrometry with tunable synchrotron radiation. Adding a large excess of O_2 to the reacting flow allows determination of products resulting from oxidation of the initial primary (R_p) and secondary (R_s) radicals formed *via* the $Cl^{\bullet}$ + DEK reaction. Because of resonance stabilization, the secondary DEK radical (3-oxopentan-2-yl) reaction with O_2 has a shallow alkyl peroxy radical (R_sO_2) well and no energetically low-lying product channels. This leads to preferential back dissociation of R_sO_2 and a greater likelihood of consumption of R_s by competing radical–radical reactions. On the other hand, reaction of the primary DEK radical (3-oxopentan-1-yl) with O_2 has several accessible bimolecular product channels. Vinyl ethyl ketone is observed from HO_2-elimination from the DEK alkylperoxy radicals, and small-molecule products are identified from β-scission reactions and decomposition reactions of oxy radical secondary products. Although channels yielding OH + 3-, 4-, 5- and 6-membered ring cyclic ether products are possible in the oxidation of DEK, at the conditions of this study (8 Torr, 550–650 K) only the 5-membered ring, 2-methyltetrahydrofuran-3-one, is observed in significant quantities. Computation of relevant stationary points on the potential energy surfaces for the reactions of R_p and R_s with O_2 indicates this cyclic ether is formed *via* a resonance-stabilized hydroperoxyalkyl radical (QOOH) intermediate, formed from isomerization of the R_pO_2 radical.

I. Introduction

As concerns over global climate change, pollution and the stability of traditional petroleum supplies continue to intensify, finding and developing alternative sources of transportation fuels have become high environmental and national security priorities.[1] As the most abundant biopolymer worldwide, cellulose has the potential to provide a major source of liquid fuels. Furthermore, because plants extract CO_2 from the atmosphere during photosynthesis, in principle their combustion can be part of a carbon-neutral cycle. However, the recalcitrance of plant material to either biochemical or thermochemical breakdown has proved to be a major impediment to efficient, large-scale production of cellulosic biofuels.[2–4]

Fungal conversion of lignocellulosic biomass is a promising new alternative to standard thermochemical and microbial decomposition methods.[5–7] The relative simplicity of fungal genomes makes these organisms useful candidates for engineering specific metabolic pathways if particular products prove to be desirable. Among the products of fungal decomposition of cellulose are a variety of ketones and other oxygenates[5,7,8] whose combustion chemistry and ignition behavior are not well understood. Novel fuels may be useful in advanced engine strategies that have the potential to combine greater efficiency and lower emissions when compared to spark ignition or diesel engines by employing autoignition of lean fuel–air mixtures.[9] Homogeneous charge compression ignition (HCCI) is a limiting case of such strategies; ignition in an HCCI engine is controlled by gas-phase chemistry, and is sensitive to the initial oxidation steps of the fuel molecule outlined in Section II.

Detecting products from the initial steps of fuel oxidation is an important foundation in an investigation of the ignition

Combustion Research Facility, Sandia National Laboratories, MS 9055, Livermore, CA 94551 USA. E-mail: cataatj@sandia.gov

† Electronic supplementary information (ESI) available: Discussion and example reactions of water elimination channels. Kinetic model (Table S1) photoionization spectra for 2-methyltetrahydrofuran-3-one, tetrahydro-4*H*-pyran-4-one and vinyl ethyl ketone (Tables S2–S4), energies, geometries and T1 diagnostic values for all stationary points calculated for Fig. 2 and 3 (Tables S5–S10) Fig. S1–S3. See DOI: 10.1039/c3cp55468f

characteristics of an individual fuel. However, such studies also provide in-depth knowledge of the fundamental reaction mechanisms involved during ignition that will enable predictive capability across a family of fuel molecules. Specifically, ascertaining the role of functional groups in the complex reactivity of particular radicals can help identify molecular structures and chemical bonding motifs that will yield desired ignition characteristics. In this study we take diethyl ketone (DEK; 3-pentanone) as a representative molecule for the family of open-chain ketones that could be harnessed from conversion of lignocellulosic feedstocks. DEK has also been investigated recently[10] as a prototype for oxidation of ketones in the troposphere, which follows many of the same channels that have been mapped out in the higher-temperature environment of autoignition.[11,12] In the present case, partially deuterated DEK isotopologs are used to investigate the various 'chain-propagating' cyclic ether + OH formation pathways from reactions of carbonyl-substituted alkyl radicals with O_2. These products are formed *via* isomerization of the initial peroxy (RO_2) radicals to hydroperoxyalkyl (QOOH) radicals that subsequently lose OH. We show that vinoxylic resonance stabilization in the QOOH is critical in directing the outcome of the reaction, and discuss possible implications for more general description of ketone autoignition.

II. Background

In the last decades investigations of fundamental oxidation chemistry have yielded a detailed mechanism for reaction pathways that govern alkane autoignition.[11,13] A simplified general mechanism is given in Scheme 1 for an initial alkyl radical (R) reacting with O_2. Formation of an alkyl peroxy radical (RO_2) typically proceeds without an energy barrier.[14,15] Of particular note in Scheme 1 is the formation of hydroperoxyalkyl radicals (QOOH) *via* internal hydrogen atom transfer from RO_2. The unimolecular decomposition of QOOH can lead to chain-propagating formation of OH, often associated with formation of a stable cyclic ether coproduct.[11,16] Alternatively, these QOOH species can promote chain-branching *via* addition of a second O_2 molecule and subsequent decomposition to two OH radicals and an oxy radical.[17] QOOH radicals have, however, never been directly detected, so observation of the stable cyclic ether products is a key indication of QOOH chemistry for any particular fuel.

In competition with QOOH formation, RO_2 can eliminate HO_2, a much less reactive species than OH. In alkane oxidation, the HO_2-elimination channel generates an alkene by removal of an H atom initially bound to a carbon neighboring the peroxy group.[14,15,18,19] Due to the relatively unreactive nature of the HO_2 radical, these channels are deemed 'chain-terminating.'[11] Understanding the overall importance of chain-propagating and chain-branching pathways relative to the chain-terminating channels facilitates prediction of the low-temperature autoignition properties of a particular compound as a fuel in advanced engines. Though larger fuel molecules have been studied,[20] the majority of compounds in which these pathways have been investigated in detail are simple hydrocarbons with more tractable mechanistic pathways.

A useful method for near-instantaneous generation of a radical pool for time-resolved study of oxidation chemistry is the pulsed-photolytic generation of $Cl^{\bullet}$ *via* photodissociation of Cl_2. The $Cl^{\bullet}$ then abstracts an H atom from the molecule of interest yielding R + HCl. However, secondary reactions involving both Cl_2 and $Cl^{\bullet}$ must also be characterized, especially if they yield products identical to those expected from oxidation chemistry. These undesired side and secondary reactions can be quenched by including sufficiently large concentrations of O_2 and fuel in the reacting flow, although experimental considerations limit the maximum practical fuel concentration. In the case of DEK, the resonance-stabilized radicals that are not as readily consumed by O_2 suffer a greater degree of secondary reactions, including chlorine chemistry. Therefore, care must be taken to identify and quantify these reactions and products so the oxidation channels can be accurately isolated and characterized.

III. Experiment

The chlorination and oxidation chemistry of DEK [$(CH_3CH_2)_2C{=}O$], d_4-DEK [$(CH_3CD_2)_2C{=}O$] and d_6-DEK [$(CD_3CH_2)_2C{=}O$] was studied at the Advanced Light Source (ALS) at Lawrence Berkeley National Laboratory. The experiment has been described in detail previously[21,22] and will only be summarized briefly here. Calibrated mass flow controllers introduce reactants and buffer gas (He) into a heated 1.05 cm i.d. quartz flow tube. The pressure in the tube is maintained at 8 Torr by feedback control of a butterfly valve in the exhaust line. The reactive mixture is continuously sampled through a ~650 μm aperture in the sidewall of the reactor. A collimated molecular beam is directed into a differentially pumped ionization chamber by passing the effluent through a 1.5 mm diameter skimmer. Quasi-continuous, tunable ionizing vacuum ultraviolet radiation provided by the ALS synchrotron intersects the molecular beam orthogonally and

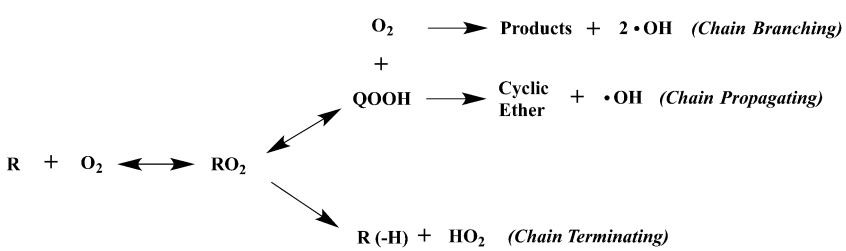

Scheme 1 Simplified mechanism for low-temperature oxidation of a hydrocarbon radical R.

Table 1 Initial concentrations (cm^{-3}) in the oxidation experiments for the compounds studied here. Helium was added to reach a total pressure of 8 Torr in all experiments

	Temp (K)	$[Precursor]_0$	$[O_2]$	$[Cl_2]$	$[Cl]_0$
DEK	550	6.6×10^{13}	2.8×10^{16}	2.9×10^{14}	8.7×10^{12}
DEK	650	5.6×10^{13}	2.4×10^{16}	2.5×10^{14}	7.4×10^{12}
d_4-DEK	550	7.2×10^{13}	2.8×10^{16}	1.5×10^{14}	4.4×10^{12}
d_6-DEK	550	7.2×10^{13}	2.8×10^{16}	1.5×10^{14}	4.4×10^{12}

Concentrations in molecule cm^{-3}.

ions are accelerated and orthogonally extracted into a linear time-of-flight mass spectrometer. Products are detected as a function of mass, time and photoionization energy yielding a 3-dimensional dataset that can be sliced and integrated to obtain photoionization spectra and temporal profiles for individual species. Photolysis of Cl_2 by a pulsed 351 nm excimer laser operating at 4 Hz yields the initial Cl• atom pool. Unless noted otherwise, concentrations of DEK, Cl_2, Cl• and O_2 are given in Table 1. A conversion of 1.5% of the Cl_2 to Cl• is estimated based on the laser fluence and the photodissociation cross section of Cl_2 at 351 nm.[23] Average pre-photolysis background signal is subtracted, resulting in difference mass spectra that show positive signal for products generated post-photolysis. Signals are normalized to the synchrotron photon flux measured by a calibrated photodiode.

Along with DEK, partially deuterated forms of DEK were obtained to isolate particular reaction pathways. The non-deuterated diethyl ketone was obtained commercially at a stated purity of >99%. The d_4- and d_6-diethyl ketone isotopologs were obtained commercially and assayed at 99.8% and 99.6% chemical purity, respectively. Vinyl ethyl ketone, 2-methyltetrahydrofuran-3-one and tetrahydro-4*H*-pyran-4-one were obtained commercially at stated purities of >95%, 98% and 99% respectively. All samples were freeze–pump–thawed to remove dissolved gases before use.

IV. Results and discussion

Vinoxylic resonance stabilization plays a key role in the oxidation chemistry of ketones, both in the formation of the initial radicals and in the isomerization pathways of the R + O_2 reactions. Chlorine-atom initiation of diethyl ketone oxidation forms both non-resonance-stabilized radicals at the primary carbons (R_p) as well as resonance-stabilized secondary radicals (R_s) (Scheme 2) for which the equilibrium R + O_2 ↔ RO_2 lies further to the left. This shift increases the likelihood that the secondary radicals will undergo other reactions besides oxidation, for example radical–radical reactions or chlorine chemistry.

Because reactions of R_s with Cl• can form vinyl ethyl ketone (VEK), which is a product of HO_2 elimination from R_pO_2 and R_sO_2, it is important to quantify to what extent these secondary chlorine reactions influence the product spectrum under our experimental conditions. The next section describes the influence of secondary chlorine reactions, and the subsequent section presents the results from oxidative chemistry.

A. Chlorine reactions

In our experiments, the photolytically generated Cl• atoms should ideally react rapidly and quantitatively with the fuel molecules. This requirement can be achieved by operating at high fuel concentration, which ensures that Cl• is dominantly consumed by reaction with the fuel and effectively suppresses secondary Cl• reactions with radical intermediates (R_p, R_s, R_pO_2, R_sO_2) and products. However in the present case, because of the efficient ionization of the ketone at the highest photon energies employed here, high DEK concentrations would unacceptably increase the total ion count rates and [DEK] was kept $\leq 7.2 \times 10^{13}$ cm^{-3} (see Table 1). Therefore the contributions of side and secondary chlorine reactions remain non-negligible and must be quantified.

The reactions of DEK and its radicals with atomic[24–27] and molecular[25] chlorine have been studied previously under a variety of temperature and pressure conditions. Fig. 1 shows current results for the time profile of DEK depletion when the concentration of Cl• immediately following photolysis is 13% of $[DEK]_0$ (Table 1). A rapid drop in DEK concentration occurs in the first ~3 ms, followed by a more gradual depletion for the extent of reaction. Hydrogen abstraction from diethyl ketone can give rise to the two distinct initial radicals defined in Scheme 2 along with calculated C–H bond dissociation enthalpies (BDE; 0 K). Unless noted otherwise, calculations presented in this work are at the CBS-QB3[28,29] level using Gaussian 09.[30] Because of the greater degree of alkyl substitution and the vinoxy-type resonance stabilization, the secondary radical (R_s) that results from abstraction of a β hydrogen is 13 kcal mol^{-1} more stable than the primary radical (R_p) originating from abstraction of a γ hydrogen. Using the bond dissociation enthalpy (BDE) of H–Cl at 0 K (102.3 ± 0.1 kcal mol^{-1}),[31] abstraction of a

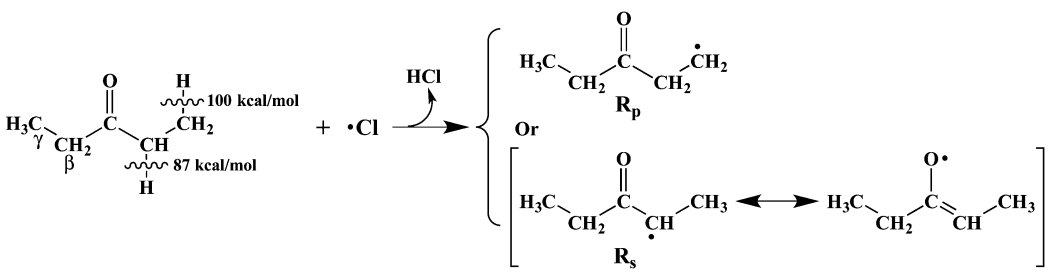

Scheme 2 H-abstraction reactions from DEK by Cl• and the resulting radicals R_p and R_s.

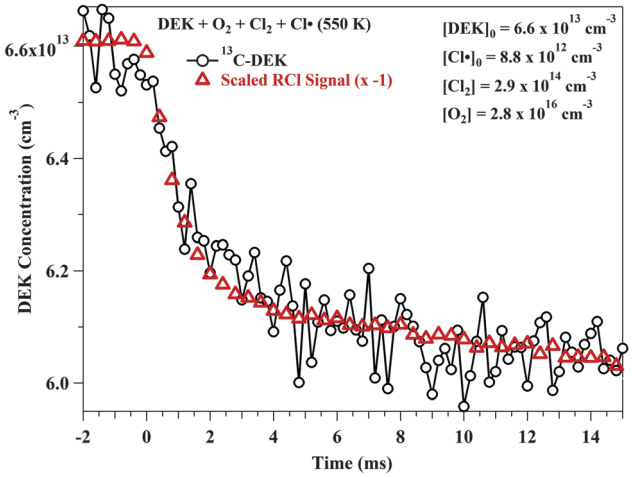

Fig. 1 Species concentration as a function of time: black circles: depletion of DEK. Red triangles: accumulation of chlorinated products 1-Cl-3-pentanone ($R_p{}^{35}Cl$) and 2-Cl-3-pentanone ($R_s{}^{35}Cl$) scaled and multiplied by −1 to show the same temporal profile as DEK depletion.

primary hydrogen to give R_p + HCl is only slightly exothermic ($\Delta H_{rxn} \approx -2$ kcal mol^{-1}), but formation of R_s + HCl is much more exothermic ($\Delta H_{rxn} \approx -15$ kcal mol^{-1}). Kaiser *et al.*[25] investigated the reactions of atomic chlorine with DEK at temperatures from 297 K to 515 K, reporting rate constants of $4.0 \times 10^{-11}\exp(-(500 \text{ cal mol}^{-1})/RT)$ cm^3 molecule^{-1} s^{-1} for primary H atom abstraction and 6.3×10^{-11} cm^3 molecule^{-1} s^{-1} for secondary H atom abstraction. These expressions are extrapolated to predict branching ratios in the present experiments: $R_p/R_s = 0.40$ at 550 K and $R_p/R_s = 0.43$ at 650 K.

The resonance stabilization of R_s is lost upon addition of O_2 and as a result the R_sO_2 well is shallow (24 kcal mol^{-1}; Fig. 2) relative to that of R_pO_2 (36 kcal mol^{-1}; Fig. 3). Because of the stability of R_s, formation of bimolecular products from R_sO_2 must proceed *via* saddle points that are above the energy of the R_s + O_2 entrance channel, which limits their importance such that back dissociation to reactants is favored. Kaiser *et al.*[25] observed the R_s + O_2 ↔ R_sO_2 equilibrium shifting towards reactants at even modestly elevated temperatures, but detected no back dissociation of R_pO_2 to R_p + O_2 up to 510 K under their experimental conditions. The temperatures of the current study are still higher (550–650 K). From the CBS-QB3 calculated equilibrium constant and the O_2 concentration in our experiments (Table 1), the equilibrium ratio $[R_sO_2]/[R_s]$ at 550 K is 0.067, while at 650 K it is only 0.002, showing that the equilibrium heavily favors the R_s + O_2 reactants at these conditions.

During the timescale of the initial reaction of Cl• with DEK, the following reactions (1–6) involving atomic and molecular chlorine can also occur (d_4-DEK is employed to highlight different isomers):

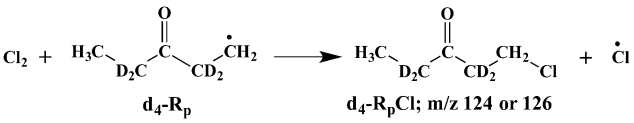

(1)

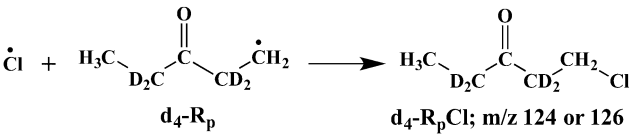

(2)

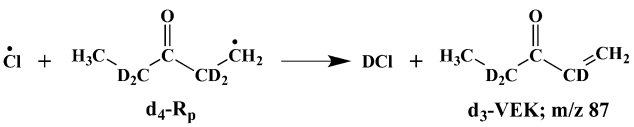

(3)

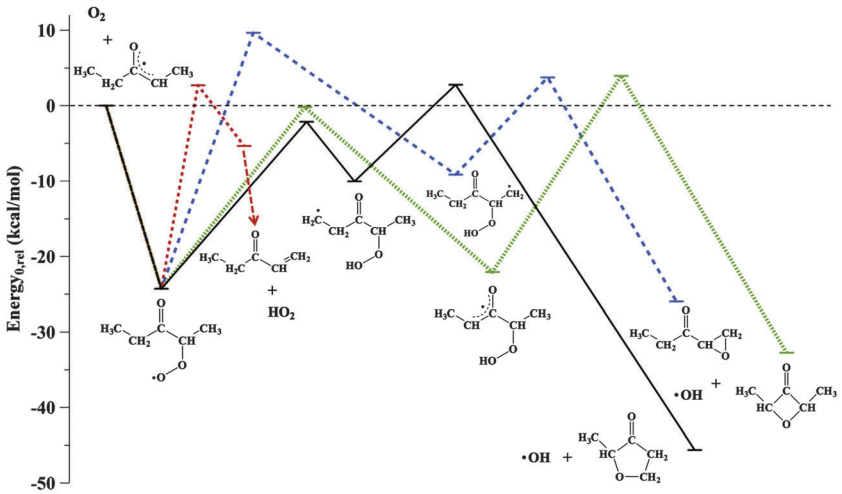

Fig. 2 Potential energy surface for the reaction of the secondary diethyl ketone radical R_s + O_2. Energies at 0 K are at the CBS-QB3 level. Several β-scission channels are also possible but for clarity are not included.

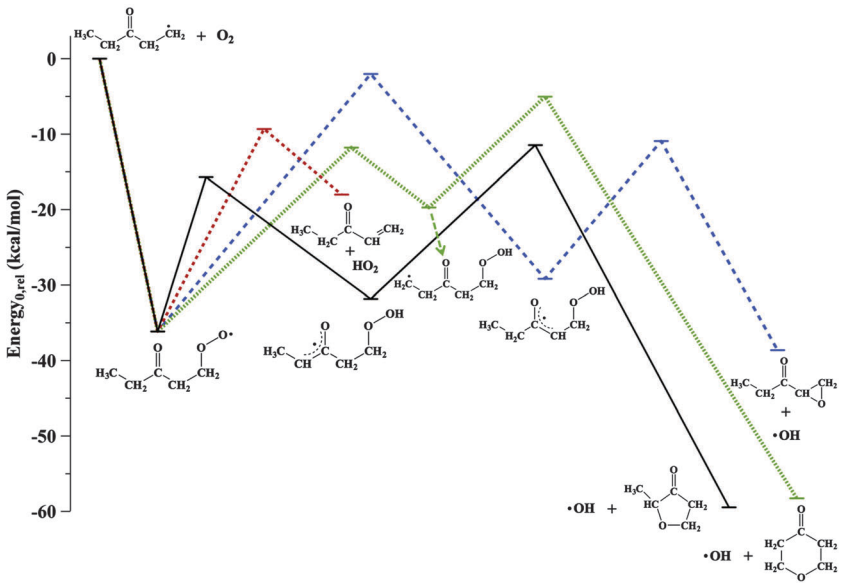

Fig. 3 Potential energy surface for the reaction of the primary diethyl ketone radical R_p + O_2. Energies at 0 K are at the CBS-QB3 level. Several β-scission channels are also possible but for clarity are not included.

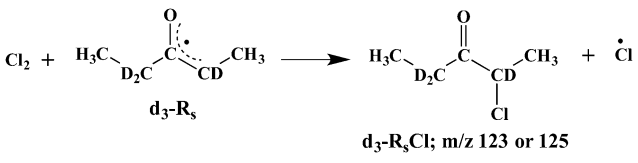

(4)

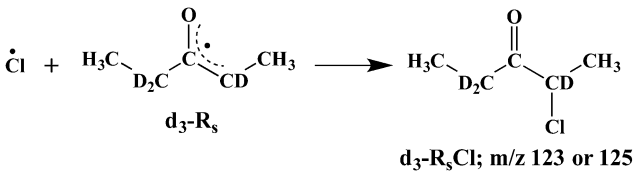

(5)

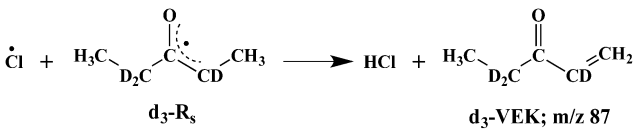

(6)

Of particular interest are reactions 3 and 6, H-abstraction or addition–elimination[32] reactions of Cl• with R_p and R_s to form vinyl ethyl ketone (VEK). Because VEK is also the product expected from the chain-terminating oxidation channel outlined in Scheme 1, accurate branching fraction determination in R + O_2 requires characterization of the Cl• + R side reactions.

The top panel of Fig. 4 shows the product mass spectrum resulting from the reaction of d_4-DEK (m/z = 90) + Cl_2 + Cl• at 550 K in the absence of O_2, measured at an ionizing photon energy of 11.0 eV. The bottom panel shows the results in the presence of O_2. In each case, both d_4-1-chloro-3-pentanone (d_4-R_pCl; m/z = 124 and m/z = 126) and d_3-2-chloro-3-pentanone (d_3-R_sCl; m/z = 123 and m/z = 125) are observed with the natural ^{35}Cl : ^{37}Cl isotope ratio. ESI,† Fig. S1 shows that the kinetic time profiles for the formation of both d_4-R_pCl (m/z = 124) and d_3-R_sCl (m/z = 123) follow the sharp depletion of the precursor d_4-DEK (Fig. 1) both in the presence and absence of O_2. The identical rise times of d_4-R_pCl and d_3-R_sCl support the interpretation that these chlorinated products largely originate from R + Cl• and not from chain chlorination in light of the vastly different chain chlorination rates of the two radicals. Kaiser *et al.*[25] report that chain chlorination reaction 1 involving R_p is nearly 150 times faster than chain chlorination reaction 4 involving R_s ($k_1 = 2.7 \times 10^{-12}$ cm^3 molecule^{-1} s^{-1} and $k_4 = 1.85 \times 10^{-14}$ cm^3 molecule^{-1} s^{-1}).

An estimate of the proportion of initial radicals that react with Cl• can be derived from comparing the amplitudes of chlorinated and oxygenated product signals as a function of O_2 concentration. Fig. 5 shows the effect of O_2 on the chlorinated product signals at 550 K taken at 11.0 eV resulting from the reaction of d_4-DEK + Cl• + Cl_2. These spectra result from integrating the ion signal over only the first 3 ms immediately following photolysis, and are dominated by the products of Cl• reactions. The red dotted curve of Fig. 5 shows chlorinated product formation in the presence of $[O_2] = 2.8 \times 10^{16}$ cm^{-3} and the black solid curve shows products in the absence of O_2. Both curves are normalized to depletion of the precursor d_4-DEK (note differing y-axis scales) and displayed so that the peak heights of the m/z = 123 feature (R_sCl) coincide. The concentration of R_sCl is found to diminish by a factor of 2.6 due to the presence of O_2, whereas R_pCl diminishes by a factor of 23.3. The greater reduction of R_pCl relative to R_sCl is consistent with rapid back dissociation of R_sO_2 and lack of low-lying R_sO_2 exit channels (Fig. 2). The introduction of $[O_2] = 2.8 \times 10^{16}$ cm^{-3} intercepts ~ 60% of R_s but > 95% of R_p.

Fig. 6 shows the ratio of cyclic ether (m/z = 100) signal to that of VEK (m/z = 84) as a function of $[O_2]$ for Cl-initiated oxidation

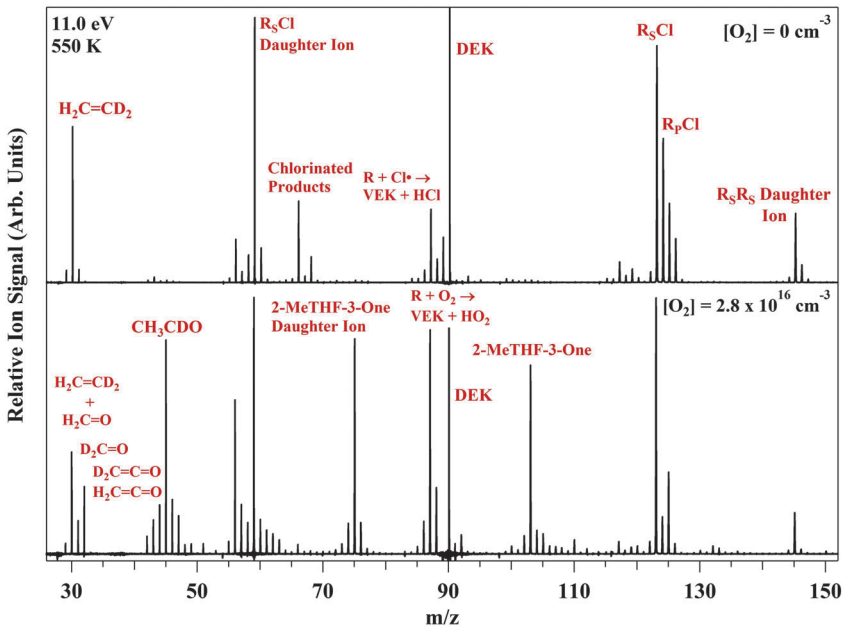

Fig. 4 Top: difference mass spectrum for the products of Cl-initiated reaction of d_4-DEK with no O_2 added to the reaction mixture at 11.0 eV. Bottom: same conditions as in the top spectrum but with an O_2 mole fraction of 0.2. Both spectra result from integrating over the first 30 ms post-photolysis.

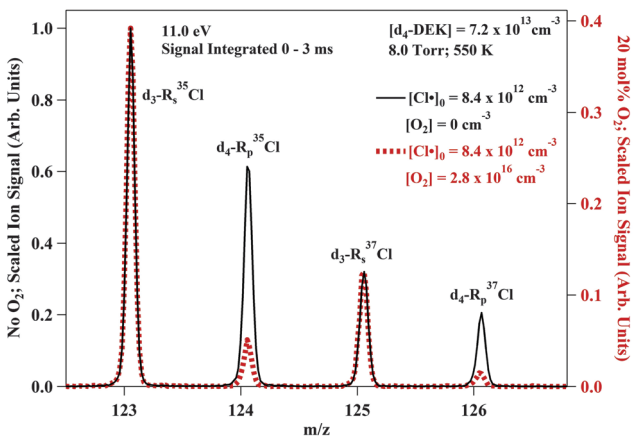

Fig. 5 Difference mass spectra for the chlorinated products observed during the 3 ms immediately following photolysis for the Cl-initiated oxidation of d_4-DEK normalized to the d_4-DEK depletion. Black solid curve: no O_2 added. Red dotted curve: 0.2 mole fraction O_2.

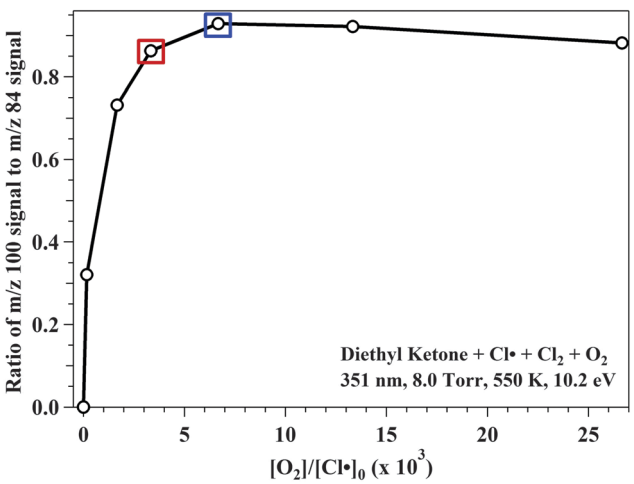

Fig. 6 Ratio of the cyclic ether (m/z = 100) signal to the vinyl ethyl ketone (m/z 84) signal in the Cl-initiated oxidation of DEK at 550 K plotted as a function of $[O_2]$ for a fixed $[Cl^•]$ of 8.8 × 10^{12} cm^{-3}. The red boxed data point indicates the $[O_2]:[Cl^•]_0$ ratio used throughout this study for DEK while the blue boxed data point indicates that used for d_4- and d_6-DEK.

of non-deuterated DEK. As expected, with no O_2 added to the reacting flow, no cyclic ether is produced and the ratio m/z = 100 : m/z = 84 is 0. As O_2 is added, the relative concentration of cyclic ether increases until reaching a plateau near a ratio of $[O_2]:[Cl^•]_0$ = 3300. At this point, the ratio m/z = 100 : m/z = 84 changes very little as a function of increasing $[O_2]:[Cl^•]_0$. To minimize the influence of secondary chlorine chemistry while maintaining sufficient signal for oxidation products, we used $[O_2]:[Cl^•]_0$ ratios of 3300 and 6600, indicated by the red and blue boxed data points highlighted in Fig. 6. However, because of the difference in reactivity of the two initial fuel radicals, the plateau in Fig. 6 does not imply that VEK yield from chlorine reactions has been eliminated. Even in the presence of $[O_2]:[Cl^•]_0$ > 3300, substantial signal is observed for R_sCl (m/z 123 and 125; Fig. 4 and 6), indicating that reaction 5 (R_s + Cl• → R_sCl) and therefore also reaction 6 (R_s + Cl• → VEK + HCl) still contribute, although reaction 2 (R_p + Cl• → R_pCl) and therefore reaction 3 (R_p + Cl• → VEK + HCl) have been effectively quenched, giving the plateau. If it were feasible to increase the fuel concentration in these experiments, higher [DEK] would reduce the role of Cl• + R reactions. However, because of its low reactivity with O_2, even at low Cl• concentrations the R_s radical is still more likely than R_p to react *via* other competing pathways, such as self reaction, rather than with O_2.

This assignment is corroborated by the observation of the R_s dimer, arising from recombination of R_s (see below).

To determine the fraction of VEK produced by chlorine reactions *vs.* HO_2-elimination, one can compare the ratio of R_pCl and R_sCl signals to VEK in the absence and presence of O_2 using d_4-DEK, where R_pCl and R_sCl molecules have different masses due to deuterium substitutions. Using the known chain chlorination rates[25] for reactions 1 and 4 and estimates for the rates of reactions 2, 3, 5 and 6, these ratios yield the VEK branching estimate. The model is detailed in the ESI† and we estimate that at the high O_2 concentrations used in this work $\sim\frac{1}{4}$ of the total VEK signal is due to reaction 6, with the remaining VEK signal arising from $R_s + O_2$ and $R_p + O_2$ reactions (see below). In the presence of O_2, reaction 3 gives a negligible contribution to VEK. Finally, reactions of $Cl^\bullet + RO_2$ to form ClO + oxy radical could also affect the interpretation of these experiments. However, peaks at 51 (^{35}ClO) and 53 (^{37}ClO) are barely discernible in our spectra, suggesting that such reactions are unimportant in these experiments.

B. Reactions of RO_2

Fig. 7 shows the product mass spectra for Cl-initiated oxidation of non-deuterated diethyl ketone (DEK) at 550 K (bottom) and 650 K (top). Major peaks are observed at m/z = 141, m/z = 122, m/z = 120, m/z = 100, m/z = 84, m/z = 72, m/z = 57, m/z = 44, m/z = 42, m/z = 30 and m/z = 28. The figure inset shows an integrated slice at higher energy (10.8–11.0 eV) demonstrating formation of ethene (C_2H_4; m/z = 28) and formaldehyde (H_2CO; m/z = 30). Peaks at m/z = 122, m/z = 120 and m/z = 57 are assigned to RCl.[25] The signal at m/z = 141 is due to a fragment ion of the R_s dimer. ESI,† Fig. S2 is an extended mass spectrum which shows

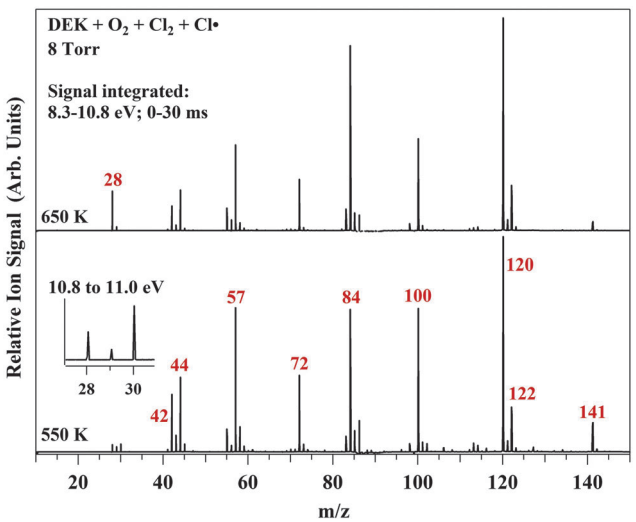

Fig. 7 Difference mass spectra of Cl-initiated oxidation of DEK at 550 K (bottom) and 650 K (top) normalized to photocurrent resulting from integrating the ion signal for the 30 ms timeframe immediately following photolysis and over ionizing photon energies from 8.3–10.8 eV. Inset: signal integrated from 10.8–11.0 eV highlighting formation of ethene and formaldehyde. Averaged background signal before photolysis has been subtracted, and negative signal arising from consumption of DEK is omitted for clarity.

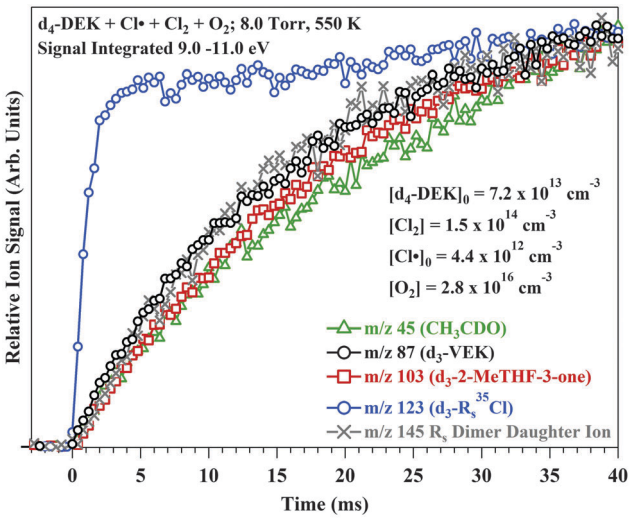

Fig. 8 Relative species concentration as a function of time for several products observed in the Cl-initiated oxidation of d_4-DEK. The chlorinated product R_sCl is observed to have a much faster rise time than the oxidation products.

that in the absence of O_2 R_sR_s and R_sR_p dimers are observed and give rise to fragment ions corresponding to loss of neutral ethyl radical. In the presence of O_2 only peaks associated with the R_sR_s dimer and its fragment remain, consistent with rapid consumption of R_p by O_2 and a significant concentration of R_s even in the presence of a large excess of O_2. Fig. 8 shows the time profiles for several products observed in the 550 K Cl-initiated oxidation of d_4-DEK, demonstrating that important oxidation products are generated on a significantly slower time scale than the rapid accumulation of chlorinated products.

i. Cyclic ether formation. The peak at m/z = 100 (Fig. 7) is assigned to cyclic ether products and serves as a marker for decomposition of QOOH radicals (Scheme 1). A number of possible pathways and cyclic ether products are available in DEK oxidation. Reactions 7 and 8 show these channels for R_p and R_s and Table 2 gives the potential products along with relative energies (0 K) and adiabatic ionization energies (AIEs) calculated at the CBS-QB3 level. The third column indicates the possible initial radical(s) that could yield the corresponding cyclic ether product. For example, the three-membered-ring cyclic ether shown in the first row, 1-(oxiran-2-yl)propan-1-one, could be formed *via* O_2-addition to R_p, followed by internal hydrogen transfer from the neighboring β carbon to yield a secondary hydroperoxyalkyl (QOOH) radical, which can then decompose to OH + cyclic ether (channel 1, reaction 7). Similarly, O_2-addition to R_s, followed by internal hydrogen transfer from the neighboring γ carbon would yield a primary QOOH and subsequently the same cyclic ether (channel 4, reaction 8).

Fig. 9a shows the photoionization spectrum for the cyclic ether products at m/z = 100 in DEK oxidation. The ionization onset near 9.1 eV matches well the calculated values for the 4- and 5-membered ring cyclic ethers shown in Table 2,

Table 2 Relative energies at 0 K ($\Delta E_{0,rel}$) of neutral cyclic ethers associated with diethyl ketone oxidation and the corresponding adiabatic ionization energies (AIEs). All energies were calculated at the CBS-QB3 level of theory

Exp. IE = 9.1 eV	$\Delta E_{0,rel}$ (kcal mol^{-1})	AIE (eV)	H-abstraction (s-secondary; p-primary)	m/z (d_0, d_4, d_6-DEK)
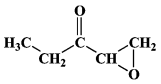	20.8	9.6	R_p, R_s	100, 103, 105
1-(Oxiran-2-yl)propan-1-one				
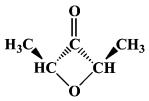	14.1 (14.3[a])	9.1	R_s	100, 102, 106
2,4-Dimethyl-oxetan-3-one				
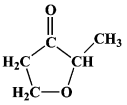	0.0	9.1	R_p, R_s	100, 103, 105
2-Me-THF-3-one				
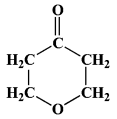	1.2	9.6	R_p	100, 104, 104
THP-4*H*-4-one				

[a] *trans* isomer.

2,4-dimethyloxetan-3-one and 2-methyltetrahydrofuran-3-one (2-MeTHF-3-one), respectively. Also shown in Fig. 9a are the standard photoionization spectra recorded for 2-MeTHF-3-one and tetrahydro-4*H*-pyran-4-one (THP-4*H*-4-one), the 5- and 6-membered ring cyclic ether products shown in Table 2 and reactions 7 and 8. The 3- and 4-membered ring cyclic ethers were not commercially available nor did we attempt to synthesize them. The photoionization spectrum of 2-MeTHF-3-one matches almost exactly that of the m/z = 100 product in DEK oxidation. No evidence of an onset in the range 9.4–9.6 eV is observed, as would be expected from a contribution from THP-4*H*-4-one or the oxirane (Table 2). Based on the results of undeuterated DEK alone, and without knowledge of the shape of the photoionization spectrum of 2,4-dimethyloxetan-3-one (4-membered ring, Table 2), formation of this compound *via* channel 5 (reaction 8) cannot be definitively eliminated from consideration.

However, studying d_4- and d_6-DEK allows separating the cyclic ether isomers by mass. The final column of Table 2 indicates the expected values of m/z for the various cyclic ether isotopologs under consideration. Based on the above discussion, we would expect to see a signal at m/z = 103 (d_3-2-MeTHF-3-one) from d_4-DEK oxidation and analogously at m/z = 105 (d_5-2-MeTHF-3-one) in d_6-DEK oxidation. In contrast, formation of the oxetane (4-membered ring) would yield products at m/z = 102 in d_4-DEK oxidation and at m/z = 106 in d_6-DEK oxidation. Fig. 9b shows the difference mass spectra for the series of diethyl ketones studied here. Both deuterated samples show a major peak at the m/z value expected from 2-MeTHF-3-one and only minor contributions at masses associated with 2,4-dimethyloxetan-3-one and THP-4*H*-4-one. Furthermore, as Fig. 9a shows, the photoionization spectra of m/z = 103 in d_4-DEK and m/z = 105 in d_6-DEK also agree well with the 2-MeTHF-3-one standard. The slight difference in shape may be due to the presence of deuterium atoms in the d_4-DEK and d_6-DEK oxidation products. Not shown in Fig. 9a are the dissociative photoionization products of 2-MeTHF-3-one and THP-4*H*-4-one. Each displays a strong fragment ion at m/z = 72. This m/z = 72 peak of 2-MeTHF-3-one has a shallow onset near 9.4 eV, and agrees well with the m/z = 72 feature observed in DEK oxidation. This feature is assigned to loss of CO from the 2-Me-THF-3-one cation. Similar features are observed at the expected masses (m/z = 75 and m/z = 77) in the oxidation spectra of d_4- and d_6-DEK. Taken as a whole, it is clear from the experimental data that one or both of the 5-membered ring cyclic ether channels of reactions 7 (channel 3) and 8 (channel 6) is dominant and thus expected to be a prominent chain-propagation mechanism in the ignition chemistry of diethyl ketone. We return to channels 3 and 6 in a discussion of computed potential energy surfaces below.

ii. HO_2-elimination. Continuing discussion in reference to Fig. 7, the m/z = 84 signal is assigned to a combination of the

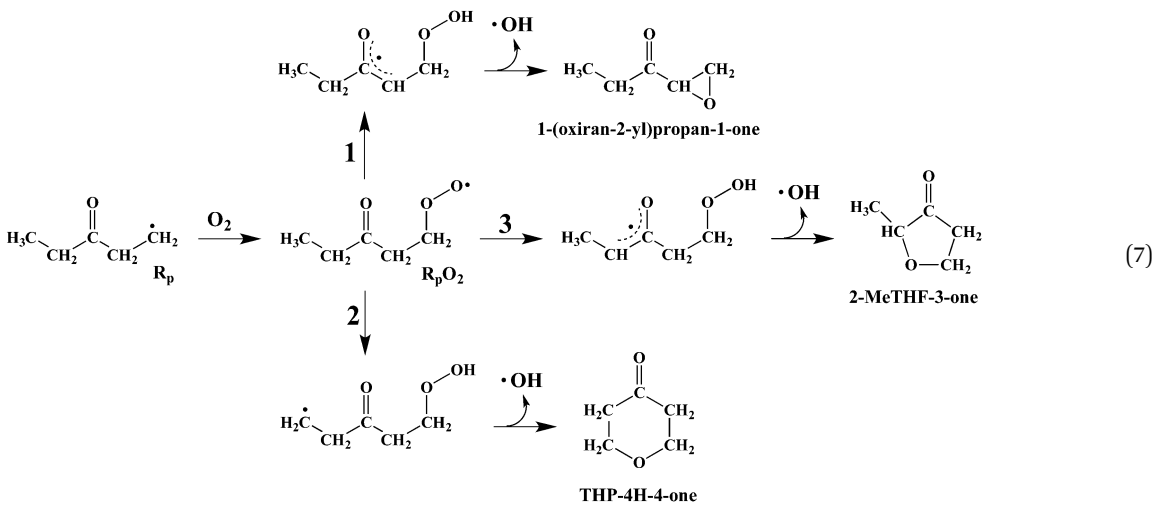

(7)

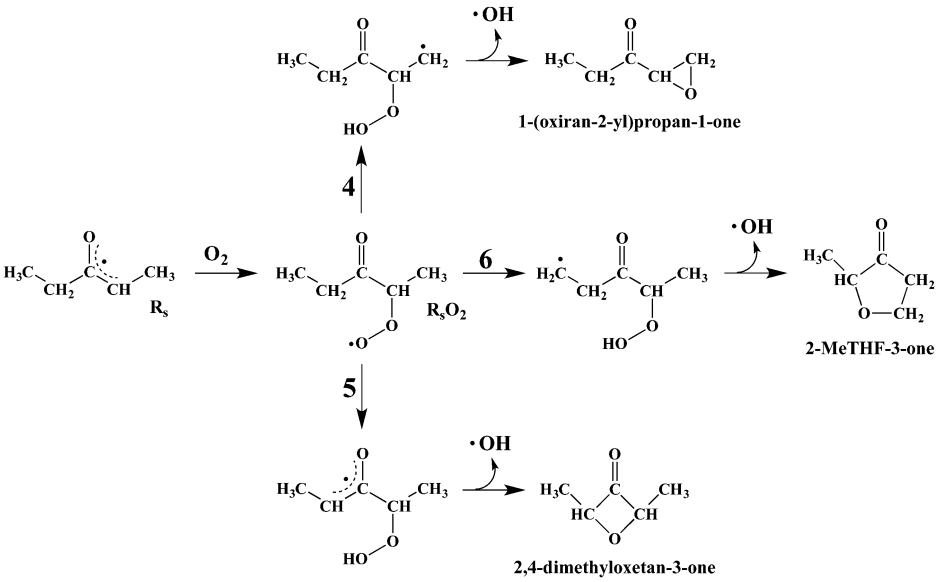

(8)

HO_2-elimination channels and reaction 6 ($Cl^{\bullet}$ + R_s). The m/z = 84 product could originate from peroxy radicals associated with either R_p or R_s (reactions 9 and 10). These channels have been investigated in a recent article discussing 1,2-acyl group migration reactions in open-chain ketones[33] and will not be discussed at length here. Briefly, the photoionization spectrum of the m/z = 84 product agrees very well with that of a vinyl ethyl ketone (VEK) standard and is given in Fig. 10, confirming the VEK assignment. Good agreement with the VEK standard is also observed for the product photoionization spectra for m/z = 87 (d_3-VEK) and m/z = 89 (d_5-VEK) in d_4- and d_6-DEK oxidation. The figure inset shows a small signal with an early onset (~8.4 eV) for m/z = 84 in DEK oxidation. This signal may be due to 3-hydroxy-penta-1,3-diene (AIE = 8.24 eV), however, its origin is unclear.

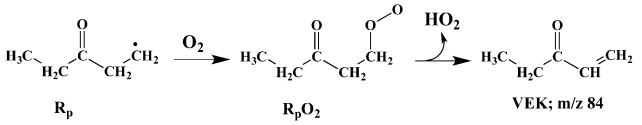

(9)

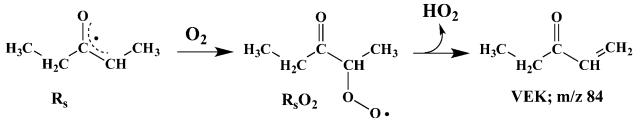

(10)

iii. Potential energy surfaces. Fig. 2 and 3 show potential energy surfaces calculated for the HO_2-elimination and cyclic ether formation channels associated with the R_s + O_2 and R_p + O_2 systems (reactions 7–10). Pathways for formation of the 3-, 5- and 6-membered ring cyclic ethers (reaction 7) as well as HO_2-elimination to form VEK (reaction 9) are all energetically plausible from R_pO_2. Note that no 4-membered ring cyclic ether is expected from unimolecular reaction of R_pO_2. Formation of 2-MeTHF-3-one from R_pO_2, is the lowest energy channel and involves a secondary, resonance-stabilized QOOH intermediate. This resonance stabilization may be expected to lower the barrier associated with the RO_2 → QOOH isomerization. However the calculated CBS-QB3 barrier (20.4 kcal mol^{-1}) is similar to that for the analogous channel in *n*-pentylperoxy calculated at the same level of theory, potentially due to increased ring strain in the R_pO_2 reaction arising from the presence of the sp^2-hybridized carbonyl carbon atom in the cyclic saddle-point structure when compared to the *n*-pentylperoxy system.[12] The QOOH associated with formation of the oxirane in Fig. 3 is also resonance-stabilized, but the degree of strain in the 5-membered ring RO_2 → QOOH transition state leads to a significantly larger barrier (34.1 kcal mol^{-1}), making this channel unfavored. In contrast to R_p + O_2, every anticipated unimolecular R_sO_2 exit channel has at least one saddle-point energy above the entrance channel (Fig. 2). Considering also that the R_s + O_2 ↔ R_sO_2 equilibrium favors reactants, it is unclear how important the pathways of Scheme 1 will be in the oxidation of R_s. All stationary point energies and geometries for the potential energy surfaces of Fig. 2 and 3 are given in ESI† along with values of the T1 diagnostic of Lee *et al.*[34] The T1 diagnostic for all structures is within the range for which single reference methods are appropriate (<0.03) with the exception of the saddle points associated with QOOH → cyclic ether + OH, which have T1 diagnostic values of 0.033–0.045. For the latter points the electronic structures are expected to have higher multireference character leading to somewhat larger uncertainties in the total energies.

C. Small molecule products

Fig. 11a–d shows photoionization spectra confirming that peaks at m/z = 28, m/z = 30, m/z = 42 and m/z = 44 in the Cl-initiated oxidation of DEK at 550 K are due to closed-shell products ethene (H_2CCH_2), formaldehyde (CH_2O), ketene (CH_2CO) and acetaldehyde (CH_3CHO). These products are also seen in d_4-DEK oxidation (Fig. 4) in which ethene is observed at m/z = 30.05 (H_2CCD_2). Formaldehyde is observed in roughly the same abundance at m/z = 30.01 (H_2CO) and m/z = 32.01 (D_2CO).

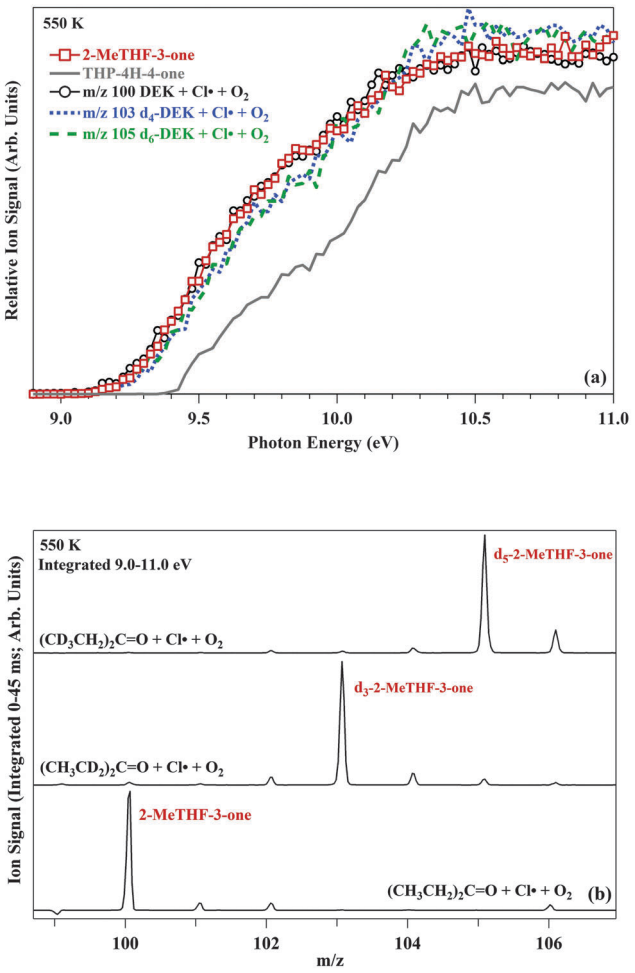

Fig. 9 (a) Photoionization spectra for the indicated peaks observed in Cl-initiated oxidation of DEK and deuterated DEK isotopologues at 550 K along with those for 2-methyltetrahydrofuran-3-one (2-Me-THF-3-one) and tetrahydropyran-4*H*-4-one (THP-4*H*-4-one) standards. (b) Product mass spectra of Cl-initiated oxidation of undeuterated DEK (bottom), d_4-DEK (middle) and d_6-DEK (top) at 550 K normalized to photocurrent resulting from integrating the ion signal for the 45 ms timeframe immediately following photolysis and over the indicated ionizing photon energies.

Ketene is observed in roughly the same abundance at m/z = 42 (H_2CCO) and m/z = 44 (D_2CCO) and acetaldehyde is observed at exclusively at m/z = 45 (CH_3CDO). Similarly, for d_6-DEK, the products are observed as follows: d_2-ethene (m/z = 30.05),

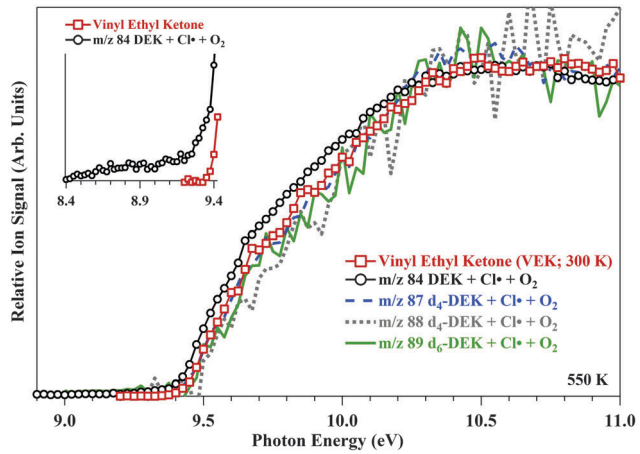

Fig. 10 Photoionization spectra for the indicated peaks observed in Cl-initiated oxidation of undeuterated DEK, d_4-DEK and d_6-DEK at 550 K compared to a VEK standard. The inset shows a minor early onset at 8.4 eV also observed at m/z = 84, possibly due to 3-hydroxy-penta-1,3-diene (calculated AIE = 8.24 eV).

d_0- and d_2-formaldehyde (m/z = 30.02 and m/z = 32), d_0- and d_2-ketene (m/z = 42 and m/z = 44) and d_3-acetaldehyde (m/z = 47; CD_3CHO). These results are summarized in Table 3 and all product photoionization spectra are included in Fig. 11. ESI,† Fig. S3 shows mass spectra of d_4-DEK oxidation in the presence and absence of O_2 in the region of ethene and formaldehyde and demonstrates the mass resolution capability of the current MPIMS experiment. No H/D atom scrambling is observed; for instance, no d_1-formaldehyde or d_1-ketene is seen in either the d_4- or d_6-DEK reactions.

The top panel of Fig. 4 shows that when O_2 is removed, ethene is still formed. This is consistent with formation *via* the R_p β-scission reaction 11, yielding ethene and propionyl radical. Propionyl is expected to decarbonylate to form ethyl radical, which will most likely add O_2 and undergo HO_2-elimination, forming an additional ethene molecule (reaction 12).[35] The first step of reaction 11 proceeds with a calculated barrier of 21 kcal mol^{-1}. Similarly, R_s can undergo β-scission reaction 13 to form methyl ketene and ethyl radical. Methyl ketene is obscured by dissociative photoionization of DEK so that we cannot quantify its formation. However, calculations indicate this reaction proceeds with a large barrier (43 kcal mol^{-1}) and is expected to be far slower than reaction 11 at 550 K.

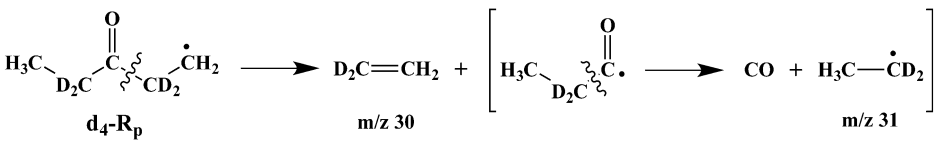

(11)

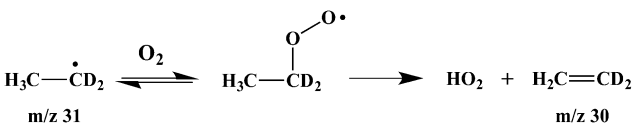

(12)

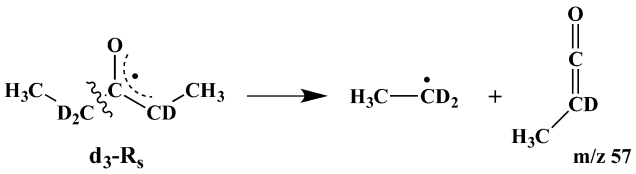

(13)

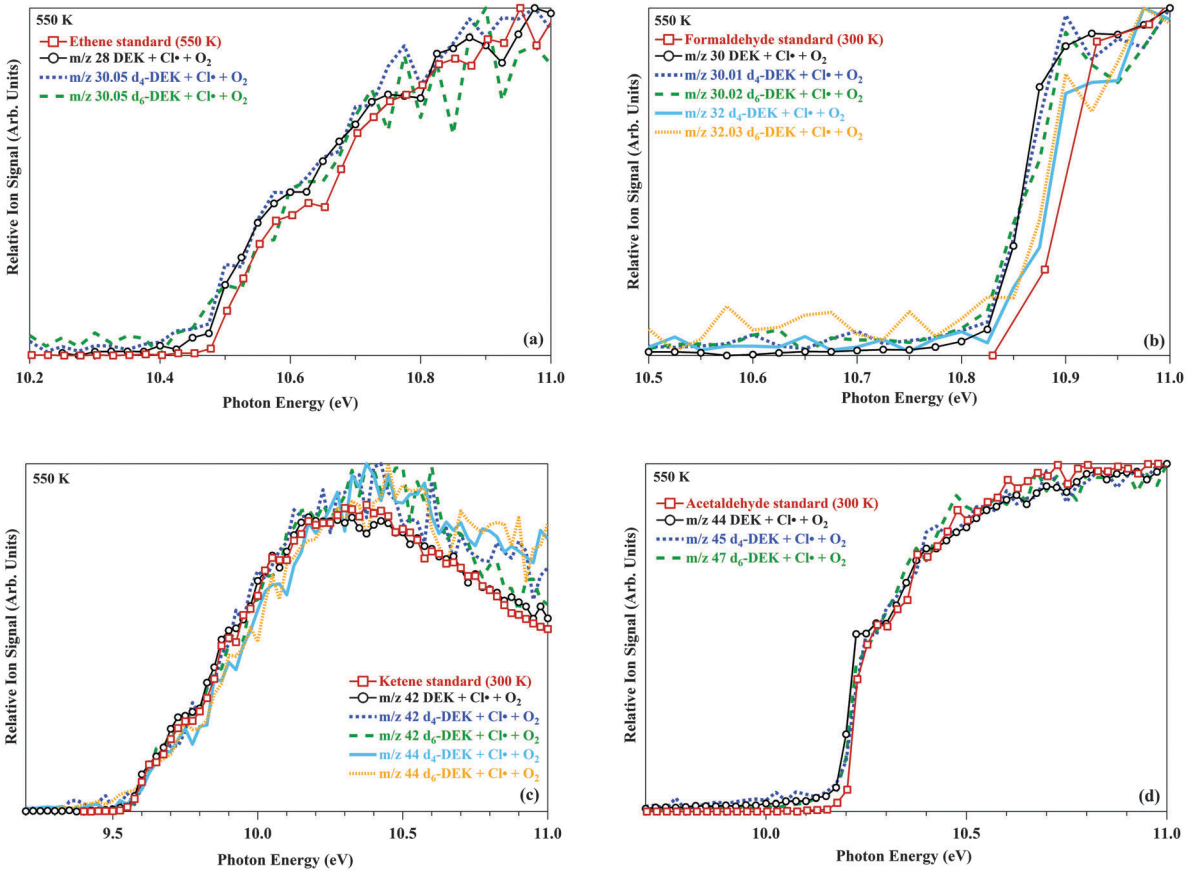

Fig. 11 Comparison of the photoionization spectra of the indicated peaks observed in Cl-initiated oxidation of undeuterated DEK, d_4-DEK and d_6-DEK at 550 K with calibration spectra (a) ethene (b) formaldehyde (c) ketene (d) acetaldehyde. The early onset observed in the acetaldehyde plot may be due to a small contribution from vinyl alcohol.

Table 3 Assignments for the small molecule products in the Cl-initiated oxidation of diethyl ketone (DEK) d_4-diethyl ketone (d_4-DEK) and d_6-diethyl ketone (d_6-DEK) at 550 K

m/z	DEK	d_4-DEK	d_6-DEK
28	H_2CCH_2		
29	CH_3CH_2 + $CH_3CH_2O_2$		
30.02	H_2CO	H_2CO	H_2CO
30.05		D_2CCH_2	D_2CCH_2
31		CH_3CD_2 + $CH_3CD_2O_2$	
32.02		D_2CO	D_2CO
32.06			CD_3CH_2 + $CD_3CH_2O_2$
42	H_2CCO	H_2CCO	H_2CCO
44	CH_3CHO	D_2CCO	D_2CCO
45		CH_3CDO	
47			CD_3CHO

Formaldehyde, ketene and acetaldehyde are formed only in the presence of O_2, and likely arise from oxy radicals formed in secondary reactions of RO_2. Self-reaction of RO_2 to yield two oxy radicals + O_2 is known to be important in many oxidative systems.[11] In the case of DEK, the resonance-stabilized R_s reacts relatively slowly with O_2 and undergoes significant side reactions, *e.g.*, dimerization both in the presence and absence of O_2. The R_s may also react with R_pO_2 to yield oxy radicals that would be expected to undergo further decomposition to generate acetaldehyde, formaldehyde and ketene, as shown in reactions 14–16 for d_4-DEK.

Self-reaction of d_4-R_pO_2 would yield two oxy radicals identical to the reactant of reaction 16. These reactions account for CH_3CDO (m/z = 45), H_2CO (m/z = 30) and D_2CCO (m/z = 44) in d_4-DEK oxidation. However, D_2CO (m/z = 32) and H_2CCO (m/z = 42) (Table 3) are still unexplained.

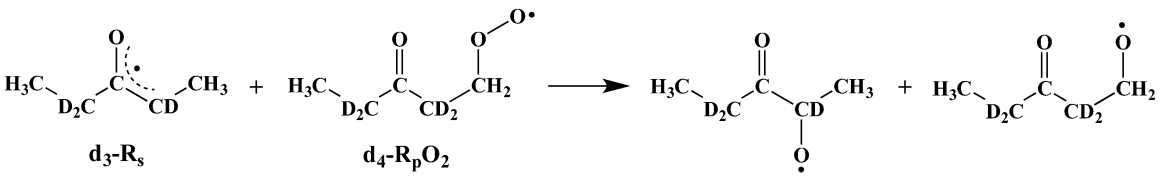

(14)

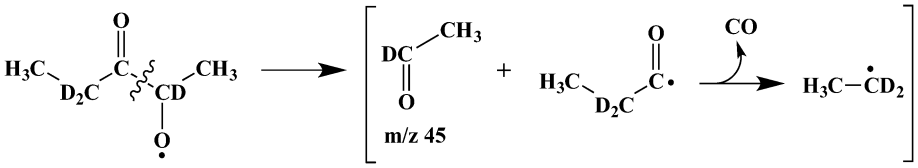

(15)

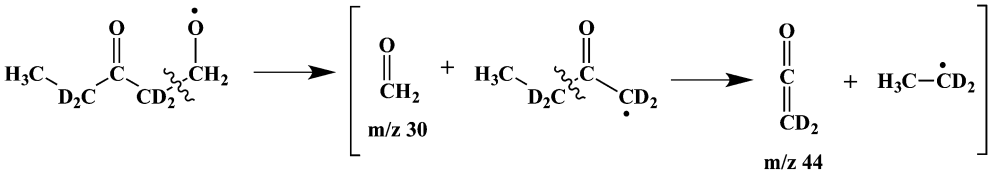

(16)

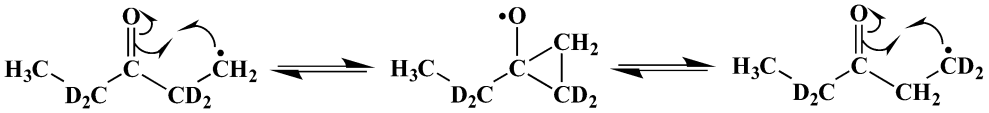

(17)

In recent work from our group,[33] the gas phase rearrangement of primary ketone radicals *via* 1,2-acyl group migration was shown to be fast relative to O_2-addition at the conditions of this study. This rearrangement is shown in reaction 17 for d_4-R_p. This rapid equilibration is expected to yield both d_0- and d_2-formaldehyde as well as d_0- and d_2-ketene *via* reactions 15 and 16.

Other possible routes for the formation of acetaldehyde appear less likely, for example, the β-scission reaction of QOOH radicals derived from R_sO_2, shown for d_4-DEK in reactions 18 and 19:

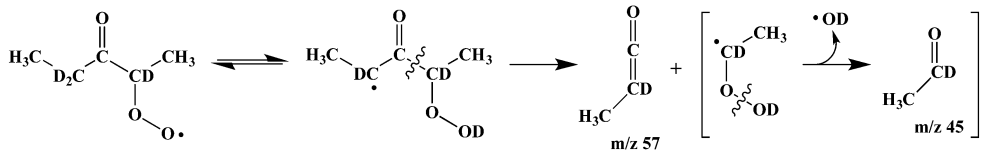

(18)

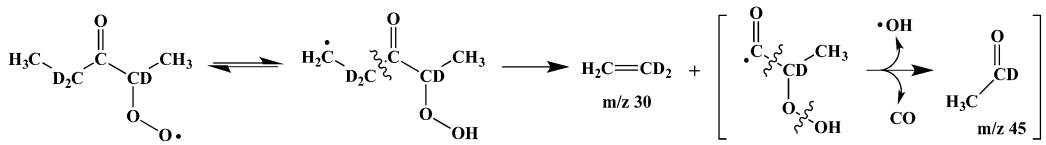

(19)

The second step of reactions 18 and 19 proceeds with calculated barriers of 33 and 22 kcal mol^{-1}, respectively. Isomerization of QOOH back to RO_2 and ring closure to form cyclic ether + OH will both be more favorable.

Recently a reaction has been characterized that involves H_2O-elimination from QOOH radicals to yield alkoxy radical co-products,[36] which in turn typically rapidly undergo unimolecular decompositions *via* β-scission. We have considered (see also ESI†) whether any similar water elimination could contribute to aldehyde and ketene formation in the DEK oxidation. However, the barrier heights are larger than 40 kcal mol^{-1} (in contrast to the ~12–17 kcal mol^{-1} barriers found for alcohols), and we conclude that water elimination does not play a significant role in the oxidation of ketones.

D. Product branching fractions

Relative product branching fractions can be determined by integrating product signals over a range of kinetic times, accounting for mass discrimination in the TOF mass spectrometer[20,37] and using previously known or currently measured photoionization cross sections of the pure compounds. The results are given for oxidation and β-scission products in Table 4. Ethene becomes the major product at 650 K, reflecting increasing dominance of β-scission reactions from the initial radicals. At 550 K, both chain-propagating OH-elimination and chain-terminating HO_2-loss are observed to be major oxidation channels, each responsible for roughly 15–20% of the quantified products as correlated by the concentrations of 2-MeTHF-3-one and VEK co-products. As shown in Fig. 3, although the barrier height for R_pO_2 → QOOH is similar to analogous saddle points in saturated hydrocarbon oxidations (20 kcal mol^{-1}), the reverse reaction of QOOH → R_pO_2 has a higher barrier (16 kcal mol^{-1}), reflecting the resonance stabilization of the QOOH. The increased

Table 4 Branching ratios determined for the products of Cl-initiated oxidation of DEK that were quantified at 550 and 650 K. Values result from integrating product signals over the 30 ms immediately following photolysis. Energies listed are the point at which the signal was compared with a standard. The standard cross sections given are at the corresponding energies. Due to error in the determination of absolute photoionization cross sections errors in the branching ratios are estimated at ±20%. Since these species do not represent a comprehensive total of all observed product signals, for ease of comparison the sums of quantified products are normalized to 1.0. The vinyl ethyl ketone branching has been adjusted to eliminate the estimated contribution from chlorine chemistry (see text)

	m/z	Assignment	Energy (eV)	Standard cross section (Mb)	Branching ratio
550 K	28	Ethene	10.80	6.19	0.10
	30	Formaldehyde	11.00	7.63	0.23
	42	Ketene	10.35	27.67	0.06
	44	Acetaldehyde	10.50	8.28	0.28
	84	Vinyl ethyl ketone	10.35	16.22	0.13
	100	2-MeTHF-3-one	10.35	9.16	0.20
650 K	28	Ethene	10.80	6.19	0.59
	30	Formaldehyde	10.83	0.7	0.07
	42	Ketene	10.35	27.67	0.02
	44	Acetaldehyde	10.50	8.28	0.13
	84	Vinyl ethyl ketone	10.35	16.22	0.12
	100	2-MeTHF-3-one	10.35	9.16	0.08

stability of the QOOH intermediate shifts the $RO_2 \leftrightarrow$ QOOH equilibrium to the right, and may favor reactions that arise from the QOOH isomer, such as unimolecular reaction to form cyclic ethers or bimolecular reaction with a "second O_2" molecule. Therefore, whereas resonance stabilization of the fuel radical R_s tends to inhibit reactivity with O_2, in the oxidation of the non-resonance-stabilized radical isomer R_p the associated resonance stabilization of the QOOH radical may tend to increase the chain propagation and chain branching pathways. This behavior will be general in the initial oxidation steps of fuels that can form both resonance-stabilized and non-resonance-stabilized radical isomers following hydrogen abstraction.

V. Conclusions

The initial reactions in the Cl-initiated oxidation of diethyl ketone and a series of deuterated diethyl ketones have been studied with multiplexed photoionization mass spectrometry using tunable synchrotron ionizing radiation. The secondary DEK radical generated by H-abstraction reactions, R_s, is resonance-stabilized and thus has a shallow well for O_2 addition, which makes the radical much less reactive with O_2 at the temperatures considered here (550–650 K).

The oxidation of DEK at 550 K yields chain-terminating HO_2 + VEK and chain-propagating OH + cyclic ether products in roughly equal abundance. A number of possible cyclic ether species are available in principle. However, nearly exclusive production of 2-methyltetrahydrofuran-3-one (2-Me-THF-3-one) is observed. This product could result from O_2-addition to either R_s or R_p. Reactions with selectively deuterated DEK allow us to rule out any significant formation of the other possible cyclic ethers. Calculated potential energy surfaces reveal that barriers to formation of oxidation products of R_sO_2 lie above the R_s + O_2 entrance channel. Conversely, the lowest energy chain-propagating pathway for decomposition of R_pO_2 is energetically favorable and proceeds *via* a resonance-stabilized QOOH to the observed 2-Me-THF-3-one product.

The small-molecule products observed provide evidence for the generation of oxy radicals from the reaction of R_s + R_pO_2 and self-reaction of R_pO_2. Observation of d_0- and d_2-formaldehyde, d_0- and d_2-ketene in both d_4-DEK and d_6-DEK provides additional corroboration of rapid 1,2-acyl group migration reactions in ketone radicals.[33]

Acknowledgements

We thank Dr John D. Savee and Dr Brandon Rotavera for useful discussions and Mr Howard Johnsen for technical support of these experiments. This work is supported by the Laboratory Directed Research and Development program at Sandia National Laboratories, a multiprogram laboratory operated by Sandia Corporation, a Lockheed Martin Company, for the United States Department of Energy (USDOE)'s National Nuclear Security Administration under contract DEAC04-94AL85000. The development of the experimental apparatus and the participation of JZ, OW, & DLO were supported by the Division of Chemical Sciences, Geosciences, and Biosciences, the Office of Basic Energy Sciences (BES), USDOE. The Advanced Light Source is supported by the Director, Office of Science, BES/USDOE, under contract DE-AC02-05CH11231 between Lawrence Berkeley National Laboratory and the USDOE.

References

1 S. Chu and A. Majumdar, *Nature*, 2012, **488**, 294–303.
2 L. R. Lynd, M. S. Laser, D. Brandsby, B. E. Dale, B. Davison, R. Hamilton, M. Himmel, M. Keller, J. D. McMillan, J. Sheehan and C. E. Wyman, *Nat. Biotechnol.*, 2008, **26**, 169–172.
3 L. R. Lynd, C. E. Wyman and T. U. Gerngross, *Biotechnol. Prog.*, 1999, **15**, 777–793.
4 M. E. Himmel, S. Y. Ding, D. K. Johnson, W. S. Adney, M. R. Nimlos, J. W. Brady and T. D. Foust, *Science*, 2007, **315**, 804–807.
5 S. K. Singh, G. A. Strobel, B. Knighton, B. Geary, J. Sears and D. Ezra, *Microb. Ecol.*, 2011, **61**, 729–739.
6 G. Strobel, S. K. Singh, S. Riyaz-Ul-Hassan, A. M. Mitchell, B. Geary and J. Sears, *FEMS Microbiol. Lett.*, 2011, **320**, 87–94.
7 G. A. Strobel, B. Knighton, K. Kluck, Y. Ren, T. Livinghouse, M. Griffin, D. Spakowicz and J. Sears, *Microbiology*, 2008, **154**, 3319–3328.
8 M. T. Mends, E. Yu, G. A. Strobel, S. Riyaz-Ul-Hassan, E. Booth, B. Geary, J. Sears, C. A. Taatjes and M. Z. Hadi, *J. Pet. Environ. Biotechnol.*, 2012, **3**, 117.
9 D. K. Manley, A. McIlroy and C. A. Taatjes, *Phys. Today*, 2008, **61**, 47–52.

10 J. D. Crounse, L. B. Nielsen, S. Jørgensen, H. G. Kjaergaard and P. O. Wennberg, *J. Phys. Chem. Lett.*, 2013, **4**, 3513–3520.
11 J. Zádor, C. A. Taatjes and R. X. Fernandes, *Prog. Energy Combust. Sci.*, 2011, **37**, 371–421.
12 A. Miyoshi, *J. Phys. Chem. A*, 2011, **115**, 3301–3325.
13 C. A. Taatjes, *J. Combust. Soc. Jpn.*, 2008, **50**, 29–38.
14 J. A. Miller, S. J. Klippenstein and S. H. Robertson, *Proc. Combust. Inst.*, 2000, **28**, 1479–1486.
15 J. J. Wilke, W. D. Allen and H. F. Schaefer, III, *J. Chem. Phys.*, 2008, **128**, 074308.
16 C. F. Cullis, A. Fish, M. Saeed and D. L. Trimm, *Proc. R. Soc. London, Ser. A*, 1966, **289**, 402–412.
17 F. Battin-Leclerc, O. Herbinet, P.-A. Glaude, R. Fournet, Z. Zhou, L. Deng, H. Guo, M. Xie and F. Qi, *Angew. Chem., Int. Ed.*, 2010, **49**, 3169–3172.
18 J. A. Miller and S. J. Klippenstein, *Int. J. Chem. Kinet.*, 2001, **33**, 654–668.
19 J. C. Rienstra-Kiracofe, W. D. Allen and H. F. Schaefer, *J. Phys. Chem. A*, 2000, **104**, 9823–9840.
20 O. Welz, J. Zádor, J. D. Savee, M. Y. Ng, G. Meloni, R. X. Fernandes, L. Sheps, B. A. Simmons, T. S. Lee, D. L. Osborn and C. A. Taatjes, *Phys. Chem. Chem. Phys.*, 2012, **14**, 3112–3127.
21 D. L. Osborn, P. Zou, H. Johnsen, C. C. Hayden, C. A. Taatjes, V. D. Knyazev, S. W. North, D. S. Peterka, M. Ahmed and S. R. Leone, *Rev. Sci. Instrum.*, 2008, **79**, 104103.
22 C. A. Taatjes, N. Hansen, D. L. Osborn, K. Kohse-Hoeinghaus, T. A. Cool and P. R. Westmoreland, *Phys. Chem. Chem. Phys.*, 2008, **10**, 20–34.
23 S. P. Sander, J. Abbatt, J. R. Barker, J. B. Burkholder, R. R. Friedl, D. M. Golden, R. E. Huie, C. E. Kolb, M. J. Kurylo, G. K. Moortgat, V. L. Orkin and P. H. Wine, *Chemical Kinetics and Photochemical Data for Use in Atmospheric Studies, Evaluation No. 17*, Jet Propulstion Laboratory, Pasadena, 2011.
24 F. Taketani, Y. Matsumi, T. J. Wallington and M. D. Hurley, *Chem. Phys. Lett.*, 2006, **431**, 257–260.
25 E. W. Kaiser, T. J. Wallington and M. D. Hurley, *J. Phys. Chem. A*, 2010, **114**, 343–354.
26 Z. Zhao, D. T. Huskey, J. M. Nicovich and P. H. Wine, *Int. J. Chem. Kinet.*, 2008, **40**, 259–267.
27 J. Albaladejo, A. Notario, C. A. Cuevas, E. Jimenez, B. Cabanas and E. Martinez, *Atmos. Environ.*, 2003, **37**, 455–463.
28 J. A. Montgomery, M. J. Frisch, J. W. Ochterski and G. A. Petersson, *J. Chem. Phys.*, 1999, **110**, 2822–2827.
29 J. A. Montgomery, M. J. Frisch, J. W. Ochterski and G. A. Petersson, *J. Chem. Phys.*, 2000, **112**, 6532–6542.
30 M. J. Frisch, G. W. Trucks, H. B. Schlegel, G. E. Scuseria, M. A. Robb, J. R. Cheeseman, G. Scalmani, V. Barone, B. Mennucci, G. A. Petersson, H. Nakatsuji, M. Caricato, X. Li, H. P. Hratchian, A. F. Izmaylov, J. Bloino, G. Zheng, J. L. Sonnenberg, M. Hada, M. Ehara, K. Toyota, R. Fukuda, J. Hasegawa, M. Ishida, T. Nakajima, Y. Honda, O. Kitao, H. Nakai, T. Vreven, J. A. Montgomery Jr., J. E. Peralta, F. Ogliaro, M. Bearpark, J. J. Heyd, E. Brothers, K. N. Kudin, V. N. Staroverov, R. Kobayashi, J. Normand, K. Raghavachari, A. Rendell, J. C. Burant, S. S. Iyengar, J. Tomasi, M. Cossi, N. Rega, N. J. Millam, M. Klene, J. E. Knox, J. B. Cross, V. Bakken, C. Adamo, J. Jaramillo, R. Gomperts, R. E. Stratmann, O. Yazyev, A. J. Austin, R. Cammi, C. Pomelli, J. W. Ochterski, R. L. Martin, K. Morokuma, V. G. Zakrzewski, G. A. Voth, P. Salvador, J. J. Dannenberg, S. Dapprich, A. D. Daniels, Ö. Farkas, J. B. Foresman, J. V. Ortiz, J. Cioslowski and D. J. Fox, Gaussian, Inc., Wallingford CT, 2009.
31 B. D. Darwent, *Bond Dissociation Energies in Simple Molecules: B. deB. Darwent*, U.S. National Bureau of Standards, 1970.
32 P. W. Seakins, E. L. Woodbridge and S. R. Leone, *J. Phys. Chem.*, 1993, **97**, 5633–5642.
33 A. M. Scheer, O. Welz, D. Y. Sasaki, D. L. Osborn and C. A. Taatjes, *J. Am. Chem. Soc.*, 2013, **135**, 14256–14265.
34 T. J. Lee, A. P. Rendell and P. R. Taylor, *J. Phys. Chem.*, 1990, **94**, 5463–5468.
35 J. D. DeSain, S. J. Klippenstein, J. A. Miller and C. A. Taatjes, *J. Phys. Chem. A*, 2003, **107**, 4415–4427.
36 O. Welz, S. J. Klippenstein, L. B. Harding, C. A. Taatjes and J. Zádor, *J. Phys. Chem. Lett.*, 2013, **4**, 350–354.
37 J. D. Savee, S. Soorkia, O. Welz, T. M. Selby, C. A. Taatjes and D. L. Osborn, *J. Chem. Phys.*, 2012, **136**, 134307.